

# Quantum Chemical Study of Point Defects in Tin Dioxide

Richard Rivera, Freddy Marcillo, Alexander Chamba,  
Patricio Puchaicela and Arvids Stashans

**Abstract** First-principles calculations based on the density functional theory (DFT) within the generalized gradient approximation (GGA), and the introduction of intra-atomic interaction term for strongly correlated *d*-electrons (DFT+*U*), have been utilized to study defective SnO<sub>2</sub> crystals. Introduction of some impurities, such as fluorine, gallium, aluminium and chromium affect the structural, electronic properties and magnetic properties of tin dioxide. F-doping produces alterations in the structure, with Sn atoms moving away from the impurity and O atoms moving closer to it; and, the system presents *n*-type electrical conductivity. Ga impurity incorporation distorts its surrounding, with the atoms moving closer to the impurity whereas the electrical properties of crystal remain unchanged. Results for Al impurity doping are almost the same as those for the Ga-doping. Cr presence produces the atoms in the neighbourhood of the point defect to move towards it, the band gap width has been slightly reduced and we observe the occurrence of a local magnetic moment.

---

R. Rivera (✉) · A. Stashans

The Grupo de Físicoquímica de Materiales, Universidad Técnica Particular de Loja, Loja, Ecuador  
e-mail: rariveraxx@utpl.edu.ec

A. Stashans

e-mail: arvids@utpl.edu.ec

F. Marcillo · A. Chamba

The Grupo de Físicoquímica de Materiales, and Escuela de Ingeniería Química, Universidad Técnica Particular de Loja, Loja, Ecuador  
e-mail: fpmarcillo@utpl.edu.ec

A. Chamba

e-mail: wachamba@utpl.edu.ec

P. Puchaicela

The Grupo de Físicoquímica de Materiales, and Departamento de Geología, Minas e Ingeniería Civil, Universidad Técnica Particular de Loja, Loja, Ecuador  
e-mail: ppuchaicela@utpl.edu.ec

**Keywords** DFT+ $U$  · Electrical conductivity · Electronic properties · Impurity doping · Microstructure ·  $\text{SnO}_2$ .

## 1 Introduction

Tin dioxide ( $\text{SnO}_2$ ) is a semiconductor oxide that crystallizes with the rutile structure. It can be described through a tetragonal crystalline lattice that belongs to the space group  $D_{4h}^{14}$  ( $P4_2/mnm$ ), in which tin atoms are in the centre of an almost regular oxygen octahedron [1, 2]. The primitive unit cell of this material is composed by two formula units (6 atoms), and the lattice parameters are  $a = 4.74 \text{ \AA}$  and  $c = 3.188 \text{ \AA}$  [1].

The stoichiometric form of  $\text{SnO}_2$  acts as an insulator, but it usually shows a non-stoichiometric form, which contains a high presence of oxygen deficiencies (tin interstitials and oxygen vacancies). These defects are responsible of its behaviour as an  $n$ -type semiconductor with a direct band-gap width of 3.6 eV [2]. The formation energy of these intrinsic point defects is reduced [3], being the reason of their high presence in this crystal.

Tin dioxide belongs to a certain type of materials that present high electrical conductivity and also a high optical transparency in the visible range of the electromagnetic spectra. These oxides are called transparent conducting oxides (TCOs). In order to understand the importance of these substances it is necessary to remember that most of electrical conductors, such as metals, are opaque; and most of the transparent solids are insulators. Hence, systems that present both characteristics are rare and have importance from both scientific and industrial point of view.  $\text{SnO}_2$  is the prototype TCO [4], because of its band-gap, width which offers up to 97 % of optical transparency in the visible range [3].  $\text{SnO}_2$  films are inexpensive, chemically stable in acidic and basic solutions, thermally stable in oxidizing environments at high temperature, and also mechanically strong. Nowadays, it is unclear the reason of the coexistence of the optical transparency alongside with the electrical conductivity, but it has been postulated that it is due the presence of oxygen vacancies [5].

The previously mentioned characteristics make TCOs suitable for applications that require the presence of electrical contacts that allow the pass of visible light [6, 7], solar energy panels, low-emission glasses, heat mirrors [8–10]. In addition, tin dioxide has some other interesting applications such as its use in sub-wavelength waveguides of ultraviolet and visible light [11], gas sensing applications [12], etc.

The nature of the properties of the  $\text{SnO}_2$  materials depend on different kind of defects and impurities that are present in the structure of this crystal. These defects could affect its structural, electronic properties, optical and/or magnetic properties. That means a strong necessity to understand the nature of the alterations being produced by the point defects in order to succeed in successful application of the tin dioxide. A large number of theoretical and experimental studies have been carried out for the pristine structure [12–16], and some other ones for the structure containing impurities [17–20]. The present work has the purpose to understand better what is

happening at the fundamental quantum level in this crystal if some impurities such as fluorine, gallium, aluminium and chromium are incorporated in the otherwise pure material.

## 2 Methodology

Density functional theory (DFT) is an approach that uses the electron density rather than Schrödinger wave function to describe a many-electron system. This method is efficient and is easily accessible; therefore, it is the choice of many research groups. Among the different computational codes that use the DFT method, Vienna *ab initio* Simulation Package (VASP) [21–24] is one of the most known and has been utilised throughout this investigation. The interactions between the core electrons and the valence electrons is implemented through the projector augmented wave (PAW) method, as it was proposed by Blöchl [25] and later adapted by Kresse and Joubert [26]. Perdew-Burke-Ernzerhof (PBE) developed [27] GGA functionals are used to describe the exchange-correlation interactions.

A cut-off kinetic energy of 500 eV is used by converging the total energy to less than 1 meV/atom.  $\Gamma$ -centred Monkhorst-Pack (MP) [28] grid with a  $0.035 \text{ \AA}^{-1}$  separation is applied, which corresponds to a  $k$ -point mesh of  $6 \times 6 \times 8$  for the 6-atom primitive unit cell of the tin dioxide. The previously mentioned parameters are obtained through the atomic relaxation until all the forces are  $<0.008 \text{ eV/\AA}$  and the equilibrium state of the system has been achieved.

DFT theory describes inappropriately strong Coulomb repulsion between the  $d$  electrons localised on metal ions. In order to take into account these issues, an unrestricted Hartree-Fock (UHF) approximation  $U$ -term has been included for the Sn- $4d$  electrons. That results in the so-called DFT+ $U$  method [29–32]. Some values for the  $U$  parameter have been tested, and finally  $U = 4.0 \text{ eV}$  was obtained as a proper magnitude for our system. The computed band-gap width was found to be equal to 1.93 eV. The corresponding experimental value is about  $3.6 \text{ eV}^2$ , but larger  $U$  values have negative impact on the equilibrium structural parameters, so we refused to enlarge the magnitude of this parameter. The computed lattice parameters have been found to be equal to  $a = 4.73 \text{ \AA}$  and  $c = 3.16 \text{ \AA}$ , in close agreement with the available experimental data [1].

Finally, in order to study the effects of fluorine, gallium, aluminium and chromium impurities in the  $\text{SnO}_2$  crystals, the 6-atom primitive unit cell was expanded sixteen times ( $2 \times 2 \times 4$  extension), which resulted in 96-atom supercell, with the corresponding  $k$ -point mesh equal to  $3 \times 3 \times 2$ .

### 3 Results and Discussion

#### 3.1 F-doped SnO<sub>2</sub>

One of the O atoms situated in the central part of the supercell was replaced by an F atom. As a result, atoms in the neighbourhood of the defective region have a tendency to displace themselves in order to find new equilibrium positions. The Sn atoms move outwards the impurity doping by approximately 0.13 Å for Sn(1), and 0.16 Å for the Sn(2) and Sn(3), meanwhile the O atoms have a tendency to displace themselves towards the impurity by 0.04 Å in case of O(5), O(6), O(7) and O(8) atoms. The value of the displacement is not the same for all O atoms since O(10), O(11), O(12) and O(13) atoms shifts only by 0.01 Å. Finally, the O(9) atom does not experience any distortion from its original site. The movements of the atoms are shown in Table 1 as well as Fig. 1.

In an attempt to explain the reason of these motions, Bader charge analysis [33] has been carried out. In this method, a robust algorithm [34–36] is employed to calculate the charge on a particular atom within the crystalline lattice. These computations show that the charge on the incorporated F atom is  $-0.76 e$ . The replaced O atom had a charge of  $-1.21 e$  in the pure crystal. This means that the tin atoms move outwards the impurity due to the reduction in the Coulomb electrostatic attraction because of the defect incorporation. Similarly, the O atoms reduce their initial distance until the F atom because of the reduction in the Coulomb repulsion. It is worth to mention that O(9) atom, which has not changed its initial distance with the defect, is the closest O atom to impurity, and has chemical bonds with Sn(3) and Sn(4) atoms. Thus, O(9) atom is trying to preserve its bond length with these tin atoms, and that explains why the distance between the impurity and the O(9) atom remains unchanged. The fact, that Coulomb electrostatic interaction is responsible for the atomic distortion

**Table 1** Atomic displacements and charges for F-doped SnO<sub>2</sub> crystal

Atom	Q1(e)	Q2(e)	$\Delta R$ (Å)
F (1)	–	–0.76	–
Sn (2)	2.41	2.43	0.13
Sn (3)	2.42	2.43	0.16
Sn (4)	2.42	2.43	0.16
O (5)	–1.20	–1.21	–0.04
O (6)	–1.21	–1.21	–0.04
O (7)	–1.21	–1.21	–0.04
O (8)	–1.20	–1.21	–0.04
O (9)	–1.21	–1.21	–
O (10)	–1.21	–1.22	–0.01
O (11)	–1.21	–1.22	–0.01
O (12)	–1.20	–1.22	–0.01
O (13)	–1.21	–1.22	–0.01

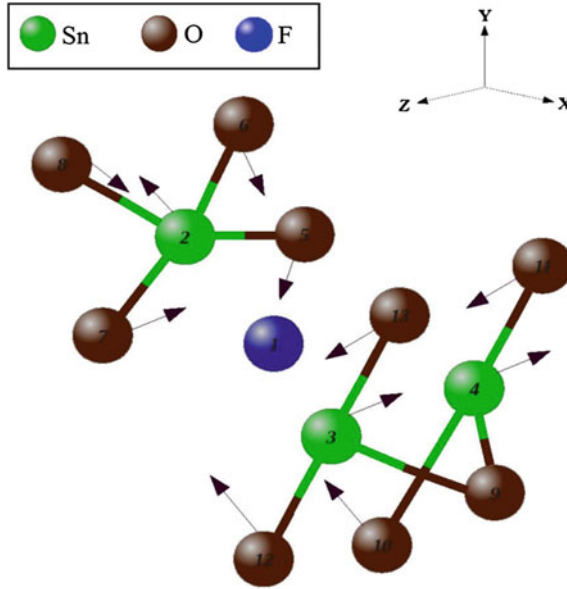


**Fig. 1** Atomic displacements in the SnO<sub>2</sub> crystalline lattice in the neighbourhood of the F-dopant. The Sn atoms move towards the impurity while the O atoms move outwards the defect

was also found in F-doped TiO<sub>2</sub>, [37] which has almost equal structure to the SnO<sub>2</sub> crystal.

Density of States (DOS) pattern for F-doped tin dioxide is shown in Fig. 2. It is possible to observe that the Fermi level has been displaced from the top of the occupied states, and now it is situated at the bottom of the conduction band (CB), which means that the introduction of the fluorine impurity, which brings to the system one extra valence electron, produces a metallic state in the CB and leads to the *n*-type electrical conductivity. That is in accordance to a number of available experimental observations [38–40].

### 3.2 *Ga-doped SnO<sub>2</sub>*

Gallium doping was done by replacing one of the lattice central host Sn atoms by the impurity. The atoms surrounding the impurity move themselves in order to find new equilibrium positions, as it is possible to see in Fig. 3. All the atoms in the neighbourhood of the impurity reduce their initial distance with respect to the

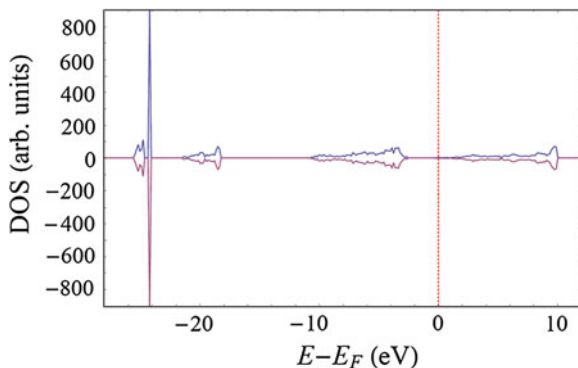


**Fig. 2** Total DOS of the F-doped  $\text{SnO}_2$  crystal. The dotted line marks the Fermi level ( $E_F$ )

**Fig. 3** Atomic displacements in the  $\text{SnO}_2$  crystalline lattice in the neighbourhood of the Ga dopant. Both Sn and O atoms have a tendency to move towards the impurity (Atomic shifts in case of the Al- and Cr-doping are essentially the same)

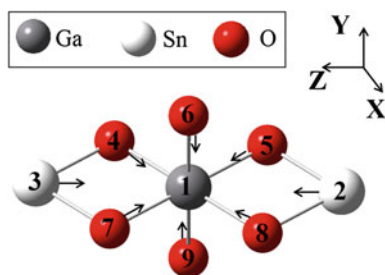


**Table 2** Atomic displacements and charges for Ga-doped  $\text{SnO}_2$  crystal

Atom	Q1(e)	Q2(e)	$\Delta R$ (Å)
Ga (1)	–	1.77	–
Sn (2)	2.42	2.43	–0.04
Sn (3)	2.42	2.43	–0.04
O (4)	–1.21	–1.17	–0.02
O (5)	–1.21	–1.17	–0.02
O (6)	–1.21	–1.16	–0.02
O (7)	–1.21	–1.17	–0.02
O (8)	–1.21	–1.17	–0.02
O (9)	–1.20	–1.16	–0.02

defect. Sn(2) and Sn(3) atoms move by 0.04 Å, and O atoms are displacing towards the impurity by 0.02 Å. Distances can be seen in Table 2.

The Bader charge analysis shows that the impurity has a charge of 1.77  $e$  instead of 2.41  $e$  for the replaced Sn atom. This means that the Coulomb repulsion force to the nearest tin atoms is smaller than that in pure crystal state, and as a consequence Sn atoms have a tendency to move closer to the dopant. O atoms move slightly closer too, most likely due to their intention to keep their bond lengths with their nearest Sn atoms, as it can be seen in Fig. 3.

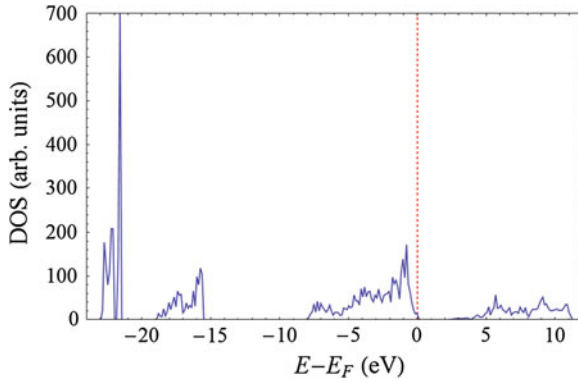


**Fig. 4** Total DOS of the Ga-doped  $\text{SnO}_2$  crystal. The dotted line marks the Fermi level ( $E_F$ )

**Table 3** Atomic displacements and charges for Al-doped  $\text{SnO}_2$  crystal

Atom	Q1(e)	Q2(e)	$\Delta R$ (Å)
Al (1)	–	2.48	–
Sn (2)	2.42	2.46	–0.07
Sn (3)	2.42	2.46	–0.07
O (4)	–1.21	–1.29	–0.09
O (5)	–1.21	–1.29	–0.09
O (6)	1.21	–1.26	–0.07
O (7)	–1.21	–1.29	–0.09
O (8)	–1.21	–1.29	–0.09
O (9)	–1.21	–1.26	–0.07

Figure 4 shows the DOS pattern for the given system. Ga atom has some small contributions in the upper valence band (VB) and the CB as well. However, there is no presence of any local energy level within the band-gap region, and no changes for the band-gap width have been detected. That means the presence of the Ga impurity in  $\text{SnO}_2$  has no notable influence upon the electrical conductivity in this material.

### 3.3 Al-doped $\text{SnO}_2$

An Al atom substituted one of the central host tin atoms in the lattice. Once the procedure of doping has been occurred, the atoms in the neighbourhood of defect start to displace themselves in order to find new equilibrium positions. The obtained relevant atomic displacements are shown in Table 3 (the movements are similar to those in the Ga-doped case, so Fig. 3 can be used to visualize the movements). It is possible to see that the nearest Sn atoms move towards Impurity doping by 0.07 Å, and most of the oxygens have a similar tendency, moving 0.09 Å, except for the O(6) and O(9) atoms, which move by 0.07 Å.

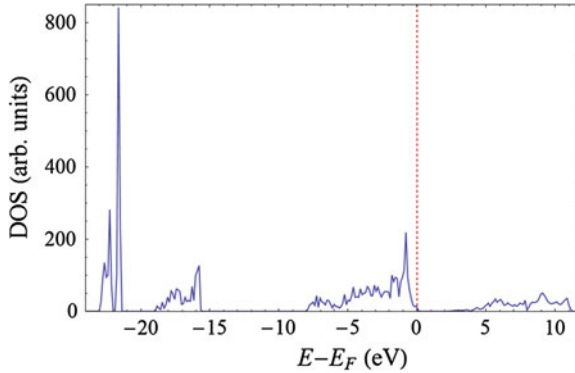


**Fig. 5** Total DOS of the Al-doped  $\text{SnO}_2$  crystal. The dotted line marks the Fermi level ( $E_F$ )

Bader charge analysis shows that the charge on the dopant atom is about  $2.48 e$ , which is slightly larger than the charge of the replaced Sn atom ( $2.41 e$ ) in undoped material. Despite small change of this atomic charge, we observe notable charge alterations on the defect-closest atoms. The tin atoms become more positive whereas the O atoms are more negative. This phenomenon means that the nature of the chemical bonding has become more ionic, which explains why the O atoms move towards the impurity. The Sn atoms try to preserve their bond lengths with the nearest O atoms, moving along with them, even if it reduces their distance regarding the dopant.

The DOS (Fig. 5) is practically unchanged due the presence of the Al atom. Impurity atom has some small contributions in the upper VB and the CB, but no presence of any local band-gap level has been observed. The band-gap width increases slightly up to  $1.78 \text{ eV}$ , which means there are no major changes on electrical conductivity.

### 3.4 Cr-doped $\text{SnO}_2$

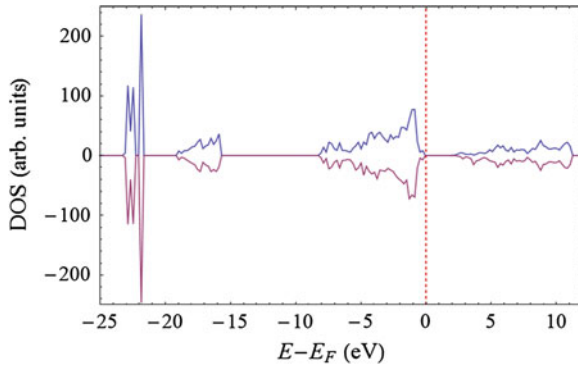
Cr-doping was done similarly to the previous cases: one of the central Sn atoms was replaced by the impurity. In order to describe appropriately the *d*electrons of the chromium impurity, parameter  $U = 4.0 \text{ eV}$  has been utilized [41, 42]. The introduction of impurity affects its surroundings with local microstructure being altered. Movements of both, Sn and O atoms are towards the impurity, and can be seen in Table 4 (atoms have moved in a similar way as in the case of Ga-doping, so Fig. 3 can be used to visualize the movements), with the closest tin atoms moving by approximately  $0.03 \text{ \AA}$  towards the impurity, and most of the O atoms displacing by  $0.06 \text{ \AA}$ , except for O(6) and O(9) atoms, which have moved  $0.09 \text{ \AA}$ .

Bader charge analysis shows that the charge on the Cr impurity is  $2.01 e$ , which is smaller than the  $2.41 e$  on the replaced Sn atom. That could explain the movements



**Table 4** Atomic displacements and charges for Cr-doped SnO<sub>2</sub> crystal

Atom	Q1(e)	Q2(e)	$\Delta R$ (Å)
Cr (1)	–	2.01	–
Sn (2)	2.42	2.47	–0.03
Sn (3)	2.42	2.47	–0.03
O (4)	–1.21	–1.16	–0.06
O (5)	–1.21	–1.16	–0.06
O (6)	–1.21	–1.13	–0.09
O (7)	–1.21	–1.16	–0.06
O (8)	–1.21	–1.16	–0.06
O (9)	–1.21	–1.13	–0.09

**Fig. 6** Total DOS of the Cr-doped SnO<sub>2</sub> crystal. The dotted line marks the Fermi level ( $E_F$ )

of the nearest Sn atoms: the Coulomb repulsion has decreased. On the other hand, it is found that O atoms also move towards the impurity. In this case, it is necessary to state that the atomic radius of the Cr atom,  $r_{Cr} = 0.615$  Å [43] is smaller than the corresponding radius of the replaced Sn atom  $r_{Sn} = 0.69$  Å [43]. That is why due to the impurity incorporation, the bond length is artificially larger than the value it should be according to the atomic radii, and the O atoms are rearranging themselves according to this fact, trying to keep an appropriate bond length with the defect, which leads to the defect-inward atomic shifts. The same effect, regarding the atomic radii, has been observed in some other researches [44–46].

DOS has been also calculated and is depicted in Fig. 6. There are no major changes upon the band structure compared to the corresponding DOS picture of the pure crystal. Nevertheless, some contributions of the Cr 3d atomic orbitals (AOs) in the CB for the  $\beta$  spin can be noticed around 4 eV above the Fermi level. The band-gap width increases slightly up to 1.85 eV.

The presence of the Cr impurity doping leads to the occurrence of local magnetic moment in the lattice. The total magnetic moment of supercell has been found to be around  $+2.0 \mu_B$ , with impurity contribution being approximately  $+2.27 \mu_B$ . Small

negative contributions of defect-nearest O atoms towards the magnetism have been also observed.

## 4 Conclusions

A quantum-mechanical study of tin dioxide ( $\text{SnO}_2$ ) in the presence of some impurities through the DFT+ $U$  approach has been carried out. The obtained structural parameters for pure crystal are in accordance with the available experimental results.

The main conclusions due to the doping of impurities can be drawn from the analysis of the obtained results. In case of the F-doping, it is found that the O atoms move towards the F atom whereas the Sn atoms move outwards the defect, due to changes in the electrostatic interaction within the defective region. Fluorine substitution leads to the increase in the  $n$ -type electrical conductivity.

The presence of a Ga impurity doping produces atomic shifts towards the defect. Neither local energy levels within the band-gap region nor changes in the band-gap width have been observed.

Al-doping changes slightly the nature of chemical bonding in its neighbourhood. It becomes more ionic due to increase of both positive and negative atomic charges on Sn and O atoms, respectively. The DOS analysis shows slight increase of the band-gap width for the doped material.

The incorporation of a Cr atom produces defect-inward atomic shifts. Cr atom itself has local influence upon the band structure properties of the material with some contributions towards the CB of material for the  $\beta$  spin. Small increase in the band-gap width is also observed. Finally, Cr dopant produces local magnetic moment in the crystalline lattice, being equal to  $+2.0 \mu_B$ .

## References

1. Yamanaka T, Kurashima R, Mimaki J (2000) X-ray diffraction study of bond character of rutile type  $\text{SiO}_2$ ,  $\text{GeO}_2$  and  $\text{SnO}_2$ . *Z Kristallogr* 215(7):424–428
2. Godinho KG, Walsh A, Watson GW (2009) Energetic and electronic structure analysis of intrinsic defects in  $\text{SnO}_2$ . *J Phys Chem* 113:439–448
3. Kiliç C, Zunger A (2002) Origins of coexistence of conductivity and transparency in  $\text{SnO}_2$ . *Phys Rev Lett* 88(9):095501
4. Lewis BG, Paine DC (2000) Applications and processing of transparent conducting oxides. *MRS Bulletin* 25(8):22–27
5. Maestre D, Ramirez-Castellanos J, Hidalgo P, Cremades A, Gonzalez-Calbet JM, Piqueras J (2007) Study of defects in sintered  $\text{SnO}_2$  by high resolution transmission electron microscopy and cathodoluminescence. *Eur J Inorg Chem* 11:1544–1548
6. Wagner JF (2003) Transparent Electronics. *Science* 300:1245–1246
7. Presley RE, Munsee CL, Park CH, Hong D, Wager JF (2004) Tin oxide transparent thin-film transistors. *J Phys D* 37(20):2810–2813

8. Zhang B, Tian Y, Zhang J, Cai W (2010) The FTIR studies on the structural and electrical properties of  $\text{SnO}_2\text{:F}$  films as a function of hydrofluoric acid concentration. *Optoelectron Adv Mat* 4(8):1158–1162
9. Moholkar AV, Pawar SM, Rajpure KY, Bhosale CH, Kim JH (2009) Effect of fluorine doping on highly transparent conductive spray deposited nanocrystalline tin oxide thin films. *Appl Surf Sci* 255(23):9358–9364
10. Kuantama E, Han DW, Sung YM, Song JE, Han CH (2009) Structure and thermal properties of transparent conductive nanoporous  $\text{F:SnO}_2$  films. *Thin Solid Films* 517(14):4211–4214
11. Sirbuly DJ, Law M, Yan H, Yang P (2005) Semiconductor nanowires for subwavelength photonics integration. *J Phys Chem B* 109,:15190–15213
12. Chaisitsak S (2011) Nanocrystalline  $\text{SnO}_2\text{:F}$  thin films for liquid petroleum gas sensors. *Sensors* 11(7):7127–7140
13. Mäki-Jaskari MA, Rantala TT (2001) Band structure and optical parameters of the  $\text{SnO}_2(110)$  surface. *Phys Rev B* 64(7):075407–075413
14. Robertson J, Xiong K, Clark SJ (2006) Band gaps and defect levels in functional oxides. *Thin Solid Films* 496(1):1–7
15. Errico LA (2007) Ab initio FP-LAPW study of the semiconductors  $\text{SnO}$  and  $\text{SnO}_2$ . *Physica B* 389(1):140–144
16. Alterkop B, Parkansky N, Goldsmith S, Boxman RL (2003) Effect of air annealing on optoelectrical properties of amorphous tin oxide films. *J Phys D* 36(5):552–558
17. Joseph J, Mathew V, Abraham KE (2007) Studies on Cu, Fe, and Mn doped  $\text{SnO}_2$  semiconducting transparent films prepared by a vapour deposition technique. *Chin J Phys* 45(1):84–97
18. Liu XM, Wu SL, Chu PK, Zheng J, Li SL (2006) Characteristics of nano Ti-doped  $\text{SnO}_2$  powders prepared by sol-gel method. *Mater Sci Eng A* 426:274–277
19. Kawamura F, Kamei M, Yasui I (1999) Effect of impurity cations on the growth and habits of  $\text{SnO}_2$  crystals in the  $\text{SnO}_2 - \text{Cu}_2\text{O}$  flux system. *J Am Ceram Soc* 82(3):774–776
20. Rivera R, Marcillo F, Chamba W, Puchaicela P, Stashans A (2013)  $\text{SnO}_2$  physical and chemical properties due to the impurity doping. Lecture notes in engineering and computer science: proceedings of the international multiConference of engineers and computer scientists. Hong Kong, pp 814–818, 13–15 Mar 2013
21. Kresse G, Hafner J (1993) Ab initio molecular dynamics for liquid metals. *Phys Rev B* 47(1):558–561
22. Kresse G, Hafner J (1994) Ab initio molecular-dynamics simulation of the liquid-metal-amorphous-semiconductor transition in germanium. *Phys Rev B* 49(20):14251–14269
23. Kresse G (1996) Efficiency of ab-initio total energy calculations for metals and semiconductors using a plane-wave basis. *Comput Mater Sci* 6(1):15–50
24. Kresse G, Furthmüller J (1996) Efficient iterative schemes for ab initio total-energy calculations using a plane-wave basis set. *Phys Rev B* 54(16):11169–11186
25. Blöchl PE (1994) Projector augmented-wave method. *Phys Rev B* 50(24):17953–17979
26. Kresse G, Joubert J (1999) From ultrasoft pseudopotentials to the projector augmented-wave method. *Phys Rev B* 59(3):1758–1775
27. Perdew JP, Ernzerhof M, Burke K (1996) Generalized gradient approximation made simple. *Phys Rev Lett* 77(18):3865–3868
28. Monkhorst HJ, Pack JD (1976) Special points for Brillouin-zone integrations. *Phys Rev B* 13(12):5188–5192
29. Anisimov VI, Zaanen J, Andersen OK (1991) Band theory and Mott insulators: Hubbard U instead of Stoner I. *Phys Rev B* 44(3):943–954
30. Solovyev IV, Dederichs PH, Anisimov VI (1994) Corrected atomic limit in the local-density approximation and the electronic structure of d impurities in Rb. *Phys Rev B* 50(23):16861–16871
31. Liechtenstein AI, Anisimov VI, Zaanen J (1995) Density-functional theory and strong interactions: orbital ordering in Mott-Hubbard insulators. *Phys Rev B* 52(8):R5467–R5470

32. Dudarev SL, Botton GA, Savrasov SY, Humphreys CJ, Sutton AP (1998) Electron-energy-loss spectra and the structural stability of nickel oxide: an LSDA+U study. *Phys Rev B* 57(3):1505–1509
33. Bader RFW (1990) Atoms in molecules: a quantum theory, the international series of monographs on chemistry 22. Oxford University Press, Oxford
34. Henkelman G, Arnaldsson A, Jónsson H (2006) A fast and robust algorithm for Bader decomposition of charge density. *Comput Mater Sci* 36(3):354–360
35. Sanville E, Kenny SD, Smith R, Henkelman G (2007) Improved grid-based algorithm for Bader charge allocation. *J Comput Chem* 28(5):899–908
36. Tang W, Sanville E, Henkelman G (2009) A grid-based Bader analysis algorithm without lattice bias. *J Phys Condens Matter* 21(8):084204
37. Stashans A, Lunell S, Grimes RW (1996) Theoretical study of perfect and defective TiO<sub>2</sub> crystals. *J Phys Chem Solids* 57(9):1293–1301
38. Zhang B, Tian Y, Zhang JX, Cai W (2011) Structural, optical, electrical properties and FTIR studies of fluorine doped SnO<sub>2</sub> films deposited by sprays pyrolysis. *J Mater Sci* 46(6):1884–1889
39. Wu S, Yuan S, Shi L, Zhao Y, Fang J (2010) Preparation, characterization and electrical properties of fluorine-doped tin dioxide nanocrystals. *J Colloid Interface Sci* 346(1):12–16
40. Elangovan E, Ramamurthi K (2005) A study on low cost-high conducting fluorine and antimony-doped tin oxide thin films. *Appl Surf Sci* 249(1–4):183–196
41. Maldonado F, Rivera R, Stashans A (2012) Structure, electronic and magnetic properties of Ca-doped chromium oxide studied by the DFT method. *Physica B* 407(8):1262–1267
42. Maldonado F, Novillo C, Stashans A (2012) Ab initio calculation of chromium oxide containing Ti dopant. *Chem Phys* 393(1):148–152
43. Shannon RD (1976) Revised effective ionic radii and systematic studies of interatomic distances in halides and chalcogenides. *Acta Crystallogr A* 32:751–767
44. Rivera R, Pinto HP, Stashans A, Piedra L (2012) Density functional theory study of Al-doped hematite. *Phys Scr* 85(1):015602
45. Patiño E, Stashans A (2001) Structural and electronic effects in BaTiO<sub>3</sub> due to the Nb doping. *Ferroelectrics* 256(1):189–200
46. Stashans A, Eras L, Chamba G (2010) Modelling of Al impurity in perovskite and ilmenite structures of MgSiO<sub>3</sub>. *Phys Chem Minerals* 37(4):191–199

Transactions on Engineering Technologies  
International MultiConference of Engineers and  
Computer Scientists 2013

Yang, G.-C.; Ao, S.-I.; Huang, X.; Castillo, O. (Eds.)

2014, X, 451 p. 145 illus., Hardcover

ISBN: 978-94-007-7683-8